Forming Limit Diagram Prediction of Tailor-Welded Blank Using Experimental and Numerical Methods

Rasoul Safdarian Korouyeh, Hassan Moslemi Naeini, and Gholamhosein Liaghat

The forming limit diagram (FLD) is a useful method for characterizing the formability of sheet metals. In this article, different numerical models were used to investigate the FLD of tailor-welded blank (TWB). TWBs were CO_2 laser-welded samples of interstitial-free (IF) steel sheets with difference in thickness. The results of the numerical models were compared with the experimental FLD as well as with the empirical model proposed by the North American Deep Drawing Research Group. The emphasis of this investigation is to determine the performance of these different approaches in predicting the FLD. These numerical models for FLD are: second derivative of thinning (SDT), effective strain rate (ESR), major strain rate (MSR), thickness strain rate (TSR), and thickness gradient (TG). Results of this research show necking will be happened, when the value of MSR, TSR, ESR criteria is maximum, TG ≤ 0.78 and SDT criterion has the first peak in forming process time. The value of dome height of TWB samples at failure was predicted based on the numerical models for samples with different widths. These numerical predictions were compared with the experimental results. The SDT model indicates a better agreement with experimental results in prediction of both the FLD and the limit dome height (LDH) in comparison to the other numerical models. Both numerical and experimental results show that minimum of LDH is happened in plane strain condition.

1. Introduction

A tailor-welded blank (TWB) consists of steels with different thicknesses, strength types welded together to produce a single blank prior to the forming process. Automotive designers are always looking for new technologies to reduce vehicle weight and manufacturing costs to meet ever restricting fuel economy standards while remaining economically competitive. An opportunity to meet these seemingly conflicting requirements is through the use of TWBs. The advantages of TWB technology can be summarized as (1) cost reduction by requiring less forming dies; (2) weight reduction by welding sheet material with different thicknesses or strengths for performance requirements; (3) part dimensional consistency improvement by removing inaccurate spot welding processes; (4) corrosion resistance enhancement by eliminating of lap joints; (5) strength improvement by substituting traditional spot welds with laser and mash seam welds (Ref 1).

The estimation of material formability plays a principal role in the design of metal forming processes. The formability of sheet metals is limited by the occurrence of localized necking, i.e., non-uniform strains within a small region in the plane of the sheet. Formability of sheet metals was experimentally characterized by the FLD according to Keeler and Backofen (Ref 2) and Goodwin (Ref 3) and later became industrial practice as well as a topic of research, both theoretically and experimentally. There are three possibilities how to determine FLD: analytical, experimental, or numerical. The forming limit of a metallic sheet is generally given in terms of the limiting principal strains under different loading conditions prior to the onset of localized necking and represented by the so-called forming limit curve (FLC). The experimental technique to determine the FLD involves subjecting specimens of sheet metal to different in-plane strain states, e.g., by simple tensile testing or stretching over a hemispherical punch. The experimental methods for determining FLDs are well established, from stretching over a hemispherical punch (Ref 4) or a circular punch with a flat bottom in Marciniak cup test (Ref 5) to biaxial stretching (Ref 2). In view of the difficulty to experimentally determine the forming limits of sheet materials, many researchers have tried to predict the FLC. FLC predictions by analytical methods were initially introduced by Swift (Ref 6) and Hill's (Ref 7) criteria under plane stress states. Later Marciniak et al. (Ref 8) introduced a criterion which is based on the presence of initial thickness heterogeneity, defined by f—the ratio of thickness of notch to thickness of bulk—in the sheet running normal to the major straining direction. They developed a numerical model to predict the localized necking and hence the forming limit for biaxial stretching of sheets.

Parallel to the time-consuming experimental approach a computer-aided numerical approach in the digital environment was developed. In 1991, Narasimhan and Wagoner (Ref 9) studied the influence of a finite groove on the plane strain intercept (FLD_0) and shape of the FLC by in-plane stretching using a finite element method (FEM) approach. They also

Rasoul Safdarian Korouyeh, Hassan Moslemi Naeini, and **Gholamhosein Liaghat**, Tarbiat Modares University, Jalal Ale Ahmad Highway, P.O. Box 14115-143, Tehran, Iran. Contact e-mail: moslemi@modares.ac.ir.

compared the predictions with the standard Marciniack-Kuczynski (M-K) model. Their researches showed that during the simulation of biaxial stretching of sheet, strain gradients within the samples grow, eventually to produce large strains within the notch corresponding to the formation of a localized neck during the actual stretching of a sheet. Narasimhan and Wagoner (Ref 9) introduced three different necking criteria based on major strain rate (MSR) (R_1), minor strain rate (R_2), and effective strain rate (ESR) (R_3) variations in the notch (or neck) and bulk region (or safe) and suggested when $R_1 \geq 4$, $R_2 \geq 10$, and $R_3 \geq 4$ necking will be happened. Brun et al. (Ref 10) suggested that the material starts to neck at the point of accelerated thinning. This phenomenon was followed by different authors (Ref 11) who determined the FLD using of numerical approach and finite element. The application of these necking criteria to understand and predict the forming limit strains of TWB is the basis of this study and will be discussed in detail later.

Many recent studies on the tailored blanks focus mainly on the formability and applications, because the FLC of the base metal may not predict the onset of necking in TWB though the failure actually occurs in the weaker material. Shi et al. (Ref 12, 13) studied the optimal conditions for laser and mash-seam welding to obtain better formability of tailored blanks. Based on experiments, they proposed that the limit thickness ratio and the limit strength ratio do not exceed the limit strain in the thin base metal. Chien et al. (Ref 14, 15) employed a bifurcation criterion to estimate the onset of failure in transversely loaded AA5754 TWBs. In their analysis, a FEM model, representing the geometrical configuration, was combined with an analytical model to predict failure. Chan et al. (Ref 16) found out that the higher the thickness ratio, the lower is the level of FLC. The findings also showed that minimum major strain decreases with increase in thickness ratio.

In this study, different numerical methods were used to predict the FLD of IF steel TWB. These methods contained: ESR, MSR, thickness strain rate (TSR), thickness gradient (TG), and second derivative of thinning (SDT) criteria to predict the forming limit of TWBs. Hill's anisotropic yield criterion and hardening model were used to model the behavior of metals. Results of numerical models were compared with the North American Deep Drawing Research Group (NADDRG) model and also with the experimental results.

TWBs were obtained by CO_2 laser welding of IF steel sheets with difference in thickness (0.77 and 1.14 mm). The experimental FLC of TWBs was determined based on the Hecker test set-up. These experimental tests were simulated using FEM to predict the FLC of TWBs by strain rate methods which were mentioned before. Dome height at failure and failure location data of TWBs from experiments and predictions were also compared.

2. Methodologies

2.1 Experimental Material and Properties

The materials used in this study are ultra-low carbon steel sheets of interstitial-free (IF) grade. These extra low carbon micro-alloyed steel sheets have been developed for application in automotive industries for highly critical body parts due to their excellent draw ability and stretch ability. The chemical composition of the steel grade used in this study is given in Table 1.

Table 2 shows the mechanical properties and forming parameters of the steel sheet studied in this work. The parameters—YS, UTS, elongation, K, and n—were evaluated by standard tensile testing of ASTM-E8 specification at 2 mm/min cross-head speed (Ref 17).

The plastic strain ratio (r), which describes anisotropy of the material in three rolling directions—r_0, r_{45}, and r_{90}—were evaluated using specimens made to ASTM-E517 specification (Ref 17). For determining the r value, specimens were elongated to 20% longitudinal strain (before the maximum load is reached). Final width and gauge length were measured and the plastic strain ratio (r) was calculated by the following equation:

$$r = \frac{\varepsilon_w}{\varepsilon_t} = \frac{\varepsilon_w}{-(\varepsilon_w + \varepsilon_l)} = \frac{\ln(w_f/w_0)}{\ln\left(l_0 w_0/l_f w_f\right)} \quad \text{(Eq 1)}$$

where w_0 and l_0 are the initial width and length, w_f and l_f the final width and length, ε_w the true width strain, ε_t and ε_l are the true thickness strain and length strain, respectively.

2.2 Fabrication of TWBs

The quality of the weld in a TWB is critical for a successful forming operation. There are many different welding processes which can be used in the welding of TWB, but laser welding and friction stair welding are two processes which are used more than others. In this study, TWBs were obtained from IF steel sheets under optimum CO_2 laser welding conditions. In this welding process no filler material was used. Parameters of CO_2 laser welding was selected such that TWB did not fail from weld zone under different forming tests. Two formability standard tests were used for investigation of weld quality: uniaxial tensile test (ASTM-E8) (Ref 17) and standard ball punch test (ASTM-E643)

Table 1 Chemical composition of steel material used for experimentation

Element	C	Si	P	S	Mn	Ni	Cr	Cu	Ti	Al
Amount, %	0.02	0.02	0.012	0.001	0.1	0.01	0.02	0.02	0.034	0.03

Table 2 Mechanical and forming properties of IF steel base metal from tensile tests

Sheet thickness, mm	YS, N/mm²	UTS, N/mm²	Elongation, %	n	K, N/mm²	Anisotropy parameter		
						r_0	r_{45}	r_{90}
0.77	156	302	47	0.25	542.4	1.94	1.8	2.73
1.17	225	340	40	0.21	616	1.81	1.64	2.54

(Ref [18]). Substandard transverse welded tensile specimens were cut from the laser-welded samples for uniaxial test. Welding power of 1.8 kW and welding speed of 1.4 m/min were selected based on the results of these two formability tests which produced good quality weld.

2.3 Numerical Investigation of TWB's FLD by FEM

Numerical investigation of stretch forming of TWBs was done using a commercially available finite element code ABAQUS 6.10. The FEM model consisted of a hemispherical punch, blank holder, die with draw bead and the blank as shown in Fig. 1. This model is based on the Hecker forming limit diagram (FLD) test (Ref [19]). Punch, die, and blank holder were modeled as an analytical rigid part, because they have negligible deformation. The blank was modeled as a deformable part by four nodes Kirchhoff thin shell elements (S4R) with shell thickness equal to the thickness of the blank. As mentioned in previous section CO_2 laser welding without any filler material was used for TWB welding in experimental tests. Laser welding produce a very narrow weld line with small heat-affected zone (HAZ), so it seems likely that the weld can safely be neglected. Therefore, the weld properties were not considered in the FEM. This assumption is also the conclusion of Saunders research (Ref [20]). The coefficient of friction at the tool-blank contact was considered as 0.15. The die was fixed and the punch was moved downward in Z-direction with a velocity of 1000 mm/s (Ref [21]).

Hill's 1948 yield criterion was used to model sheet metal behavior in forming process (Ref [22]).

$$f(\sigma) = \sqrt{F(\sigma_{22} - \sigma_{33})^2 + G(\sigma_{33} - \sigma_{11})^2 + H(\sigma_{11} - \sigma_{22})^2 + 2L\sigma_{23}^2 + 2M\sigma_{31}^2 + 2N\sigma_{12}^2} \tag{Eq 2}$$

$$F = \frac{1}{2}\left(\frac{1}{R_{22}^2} + \frac{1}{R_{33}^2} - \frac{1}{R_{11}^2}\right), \quad G = \frac{1}{2}\left(\frac{1}{R_{33}^2} + \frac{1}{R_{11}^2} - \frac{1}{R_{22}^2}\right),$$

$$H = \frac{1}{2}\left(\frac{1}{R_{11}^2} + \frac{1}{R_{22}^2} - \frac{1}{R_{33}^2}\right),$$

$$L = \frac{3}{2R_{23}^2}, \quad M = \frac{3}{2R_{31}^2}, \quad N = \frac{3}{2R_{12}^2} \tag{Eq 3}$$

F, G, H, L, M, and N are the Hill's criterion coefficients. These coefficients can be imported into the software by 6
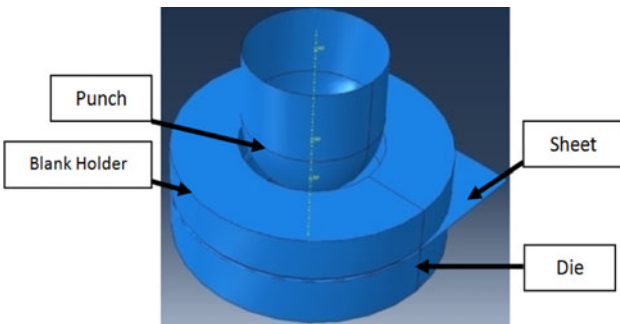

Fig. 1 Modeling in ABAQUS software

yield stress parameters of R_{11}, R_{22}, R_{33}, R_{12}, R_{13}, and R_{23}. These parameters can be calculated using anisotropic parameters of r_0, r_{45} and r_{90} as fallows (Ref [23]).

$$R_{11} = R_{13} = R_{23} = 1, \quad R_{22} = \sqrt{\frac{r_{90}(r_0 + 1)}{r_0(r_{90} + 1)}},$$

$$R_{33} = \sqrt{\frac{r_{90}(r_0 + 1)}{r_{90} + r_0}}, \quad R_{12} = \sqrt{\frac{3r_{90}(r_0 + 1)}{(2r_{45} + 1)(r_{90} + r_0)}} \tag{Eq 4}$$

The stress-strain relation for strain hardening of the materials during plastic deformation was considered by Hollomon constitutive equation:

$$\sigma = K\varepsilon^n \tag{Eq 5}$$

where σ is the flow stress, ε is true strain, K is the strength coefficient, and n is the strain hardening coefficient.

The standard eight different strain paths (25×200 to 200×200 mm) were simulated to predict the FLD of welded blank. Limit strains were obtained using a few necking criteria which is explained in next sub-section. Optimal blank holder force (20 to 60 kN) was chosen such that the blank neither draws-in nor tears near draw bead.

2.4 Necking Criterion for FLD Prediction in FEM

In this study, six different necking criteria were used to investigate their applicability in predicting the forming limit of TWBs. These necking criteria are described below.

2.4.1 SDT Criterion. As mentioned before, material thinning can be a criterion for necking. Using Brun's idea, time, and spatial necking of a particular specimen can be predicted based on the SDT (Ref [10], [11]). Based on this model, thickness of all elements of FEM workpiece was analyzed to determine minimal thickness for each stored time interval. Thinning values of all elements which has minimal thickness was stored. Finally, SDT in time was analyzed. Due to a fast local change of sheet thickness at the necking point the thickness strain leaping changes its value. The acceleration of thickness deformation (second time derivative) is defined as

$$\ddot{\varepsilon}_{33} = \frac{d^2\varepsilon_{33}}{dt^2} \tag{Eq 6}$$

where ε_{33} is the thickness strain of element. The element at which the peak of $\ddot{\varepsilon}_{33}$ first appears (at minimal time) was assumed as the element where the onset of necking started and the time of this peak was considered as necking time.

Selected elements from each specimen's geometry based on this method were considered to be at the necking point of the analyzed material. The major and minor strains for these elements were collected from the Abaqus result file and put into the FLD diagram. Figure 2 shows SDT for critical element in 25×200 and 200×200 mm strain paths. Minimum of $\ddot{\varepsilon}_{33}$ for 25×200 mm strain path was happened in 0.04 s and for 200×200 mm strain path in 0.038 s. This time difference

for minimum of SDT cause variation of their major and minor strains and this trend is occurred for other strain paths. FLD based on SDT was formed using major and minor strains which were identified by this model for all strain paths.

2.4.2 ESR Criterion. ESR is the ratio of ESR in the neck to that in the safe region (or bulk). ESR increases unstably during the necking process.

$$\text{ESR} = \frac{\text{Effective strain rate in the neck region}}{\text{Effective strain rate in the safe region}}$$

As mentioned before other researcher's results show when ESR $\geq$ 4 necking will happen (Ref 9), but results of present research for TWB show when ESR is maximum necking will be happened. In the present investigation at first element with minimal thickness (element which necking will start to happen from it firstly) was identified. By considering side element of this element as safe region, ESR for this element was calculated for all the forming process time. Maximum value of ESR and its time was determined and major and minor strain of safe element at that time was put into the FLD diagram. This procedure was repeated for all specimens which were considered for FLD determination in FEM. Figure 3 shows changes of ESR with true major strain in safe region for 50×200 and 200×200 mm strain paths. By considering
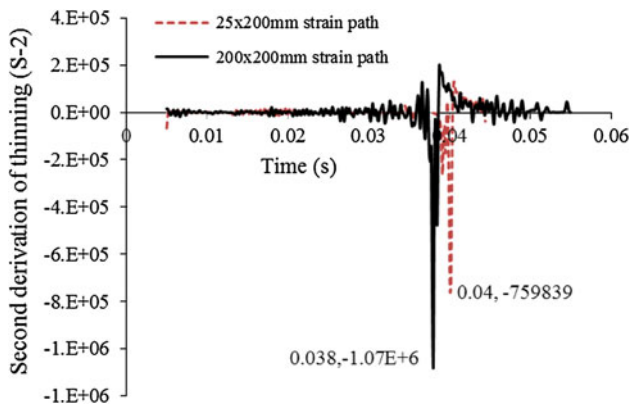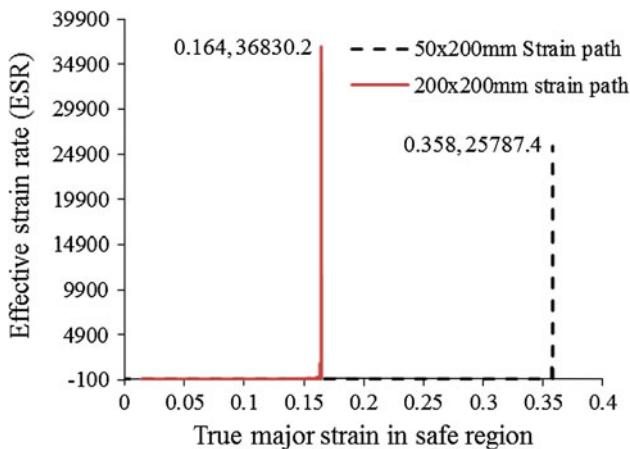
of minor strains of these two strain paths, two points for the left-hand side (from 50×200 mm strain path) and right-hand side (from 50×200 mm strain path) of FLD is obtained.

2.4.3 MSR Criterion. MSR is the ratio of major principal strain rate in the neck to that in the safe region. MSR increases unstably during the necking process.

$$\text{MSR} = \frac{\text{Major strain rate in the neck region}}{\text{Major strain rate in the safe region}}$$

Previous researcher's results show when MSR $\geq$ 10 necking will happen (Ref 9). Results of present research for TWB with different thicknesses show when MSR is maximum, necking will be happened. MSR was calculated for minimal thickness element of specimens in a procedure like ESR for all the forming process time. When MSR was maximum, major and minor strains of the bulk element was considered as a point of FLD. Variations of MSR with true major strain of safe region for 50×200 and 150×200 mm strain paths is shown in Fig. 4.

2.4.4 TSR Criterion. TSR is the ratio of TSR in the neck to that in the safe region. TSR increases unstably during the necking process.

$$\text{TSR} = \frac{\text{Thickness strain rate in the neck region}}{\text{Thickness strain rate in the safe region}}$$

TSR and its FLD points were calculated similar to the previous strain rate criteria (ESR, MSR). When TSR is maximum
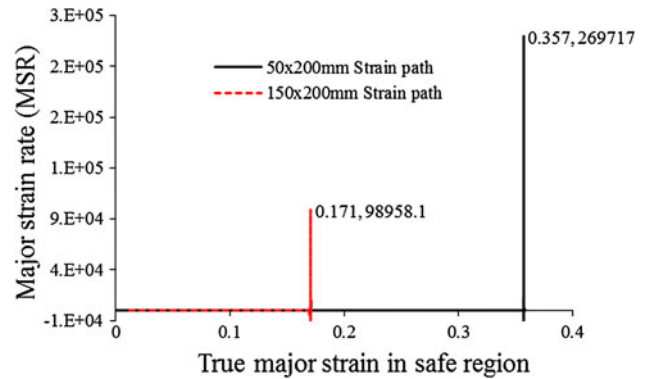

Fig. 2 SDT for critical element at 25×200 and 200×200 mm strain paths

Fig. 4 Variation of MSR ratio with true major strain in safe region for 50×200 and 150×200 mm strain paths

Fig. 3 Variation of ESR ratio with true major strain in safe region for 50×200 and 200×200 mm strain paths
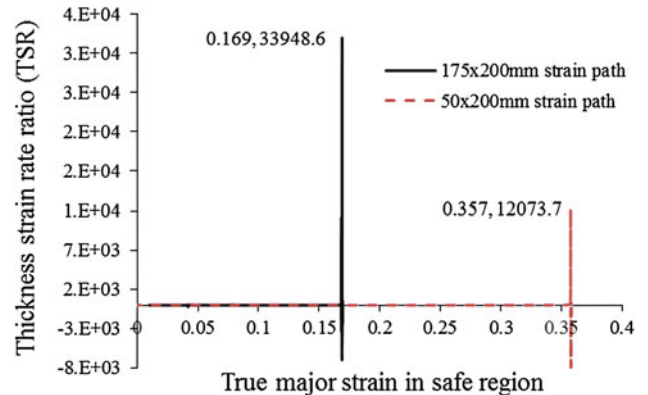

Fig. 5 Variation of TSR ratio with true major strain in safe region for 50×200 and 175×200 mm strain paths

necking will be happened. Variations of TSR with true major strain of safe region for 50×200 and 175×200 mm strain paths are shown in Fig. 5.

2.4.5 TG Criterion. In the Marciniack-Kuczynski (M-K) criterion necking was predicted when the ratio of the thickness of necking region to the bulk reaches a critical magnitude. A new failure criterion was suggested by Kumar et al. (Ref 24) based on M-K necking criterion. This new criterion was represented as follow:

$$TG = \frac{\text{Current thickness of notch}}{\text{Current thickness of bulk}} \leq C$$

The magnitude of C was determined experimentally by measuring the TG across the localized necks in a few tensile samples. In the present research, three samples of transverse IF TWB with 10 mm width and 200 mm length were deformed under tensile loading until a neck just begins to initiate. Thickness variation of samples in direction perpendicular to the neck was measured by micrometer and is shown in Fig. 6. As expected, the thickness decreases and then increases across the neck. All the three flat sheet samples show similar behavior.

It can be seen from Fig. 7 that the thickness ratio across the neck reaches a critical magnitude of 0.78 at the onset of necking. The value of C was therefore selected as 0.78 for FEM. Hence, in the present simulations, element pairs where the thickness ratio equals or falls below 0.78 first are considered as necked elements. When $C \leq 0.78$ the major and minor strains in the thicker element (safe region) are then described as the forming limit strains of that particular deformation condition. Figure 8 shows variation of TG for 25×200 and 200×200 mm strain paths with time.
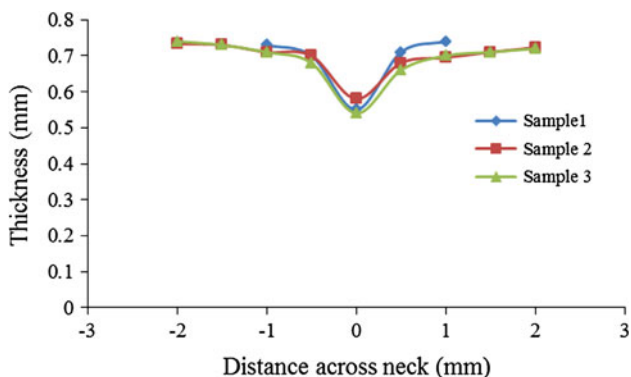

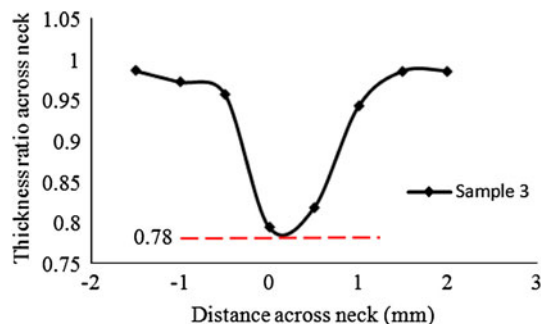**Fig. 6** Variation of thickness across the neck

Fig. 7 Variation of thickness ratio between adjoining elements across the neck

2.4.6 NADDRG Criterion. For simplifying the experimental and theoretical determination of the FLD, the NADDRG introduced an empirical equation (Ref 25). According to this model, the FLD is composed of two lines through the point FLD_0 in the plane-strain state. The slopes of the lines located, respectively, on the left- and the right-side of the FLD are about 45° and 20°.

$$t \leq 2.54 \text{ mm}, \quad FLD_0 = \frac{n}{0.21}(23.3 + 14.13t) \quad \text{(Eq 7)}$$

where t is thickness of sheet, n is work hardening power, and FLD_0 is a point on the major strain axes and is minimum point of FLD.

FLD of thinner part of IF TWB was calculated using Table 2 and NADDRG model and was imported as FLD of TWB in Abaqus software.

2.5 Experimental Setup for FLD

The biaxial stretch-forming tests were done according to the procedure suggested by Hecker (Ref 19) using a hemispherical punch of 101.6 mm diameter on a 20 tones hydraulic press. The setup of the tool arrangement (punch, lower die, and upper die) used in the experiments is shown in Fig. 9.

A circular draw bead was provided on the die with 132 mm diameter to restrict the flow of metal from the flange region into the die and to ensure that only the portion within the die
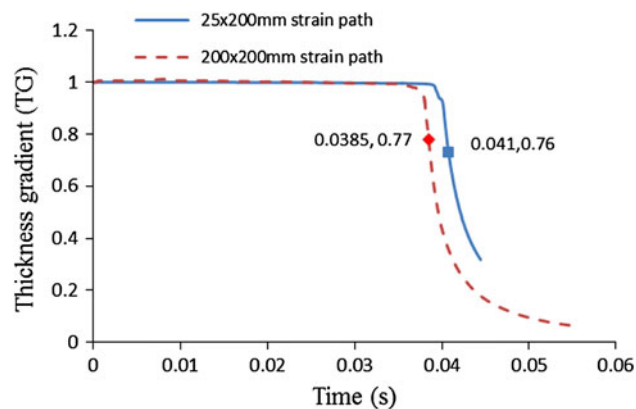

Fig. 8 Variation of TG with time for 25×200 and 200×200 mm strain paths
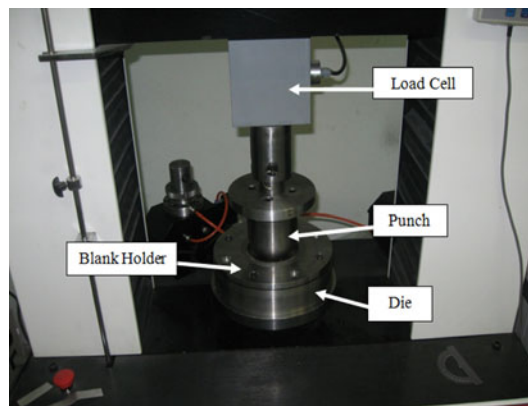

Fig. 9 Experimental FLD setup

opening was deformed by the punch. All the tests were conducted in dry condition at a punch speed of 20 mm/min. An optimum blank holding force in the range of 6-10 tones was applied on the upper die for specimens with different widths. A shim sheet with 0.4 mm thickness was used on the thinner side of TWB and hence uniform blank holding pressure was obtained throughout the blank. The press was equipped to load and displacement sensors and experiments were stopped when forming load decrease suddenly.

Eight specimens of size 25 × 200 to 200 × 200 mm were cut from the laser-welded specimen such that weld line were perpendicular to the stretching direction (transverse specimens). Specimens were grid marked with circles of 2.5 mm by electrochemical etching method to measure major and minor strains after deformation. Figure 10 shows the series of specimens used in this experiment.

The circles on the sheet samples became ellipses after deformation, falling into safe, necked, and failed zones. The principal strains in the plane of the sheet were expressed using the true strain measures. The true major and minor strains were calculated by measuring change of the principal directions, a and b, of the ellipse with reference to the initial diameter, d_0, of the circle

$$\varepsilon_{major} = \ln\left(\frac{a}{d_0}\right), \quad \varepsilon_{minor} = \ln\left(\frac{b}{d_0}\right) \tag{Eq 8}$$

where a and b are the ellipse diameters and d_0 is the initial diameter of circle. FLD was drawn by separating the safe-limiting strains from the unsafe zone containing the necked and fractured ellipses.

3. Results and Discussion

3.1 Formability and Microstructure of IF TWB

As mentioned before, for choosing correct welding parameters two formability tests of ASTM-E8 and standard ball punch were done. Figure 11 shows a transverse TWB sample after uniaxial tension (ASTM-E8) which is an in-plane tension
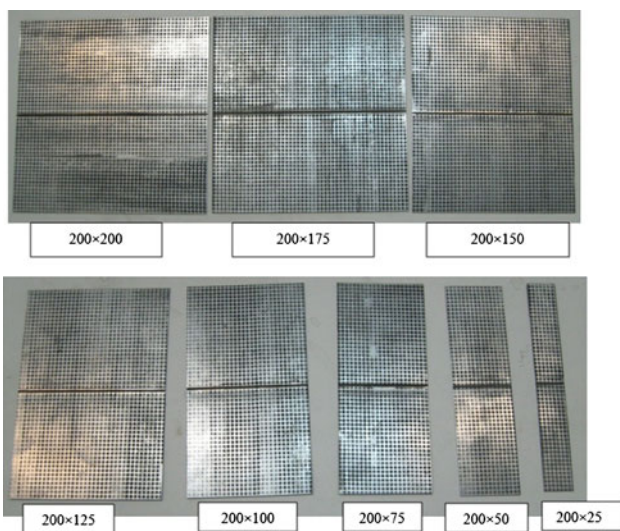
test. Necking happened in the thinner side of TWB and far from weld line.

Result of standard ball punch test which is an out of plane formability test is shown in Fig. 12. In this test also necking happened in the thinner side of TWB and parallel to the weld line.

In both in-plane and out of plane tests, fracture was happened in the thinner side of TWB and weld line was safe. Results of these tests show that welding parameters were selected correctly and these parameters were used for welding of FLD samples. Figure 13(a) shows the microstructure of IF steel sheet. Ferrite grains can be seen in this figure. Figure 13(b) shows the microstructure of IF TWB. The microstructure of the three zones (parent metal, HAZ, and the weld region) is shown in Fig. 13(b). Significant grain growth is
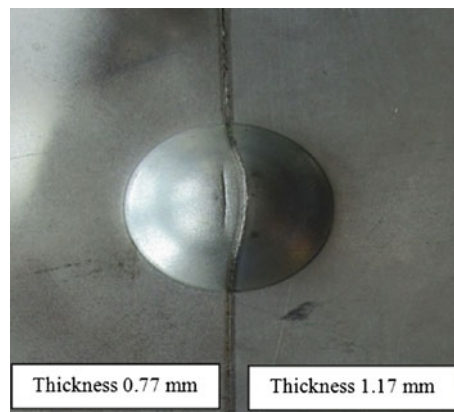

Fig. 11 TWB sample after ASTM-E8 test

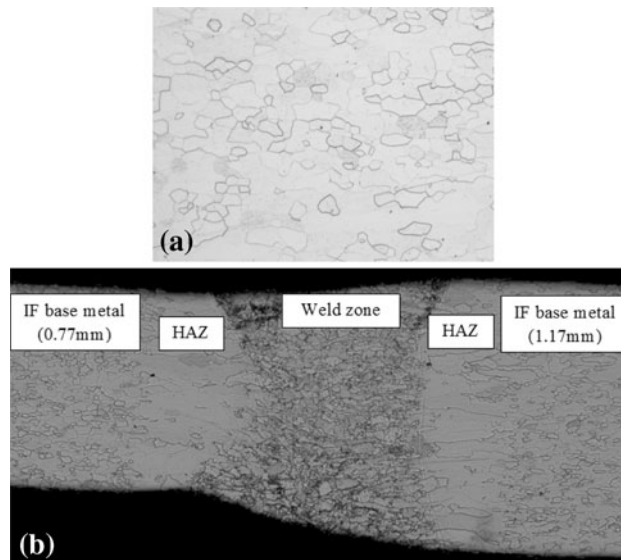**Fig. 12** Necking position in the standard ball punch test

Fig. 13 Microstructure of (a) IF steel sheet—200×—Nital etched, (b) IF TWB—200×—Nital etched

Fig. 10 A series of TWB specimens

observed in the HAZ region. In the weld zone, the grains are of irregular shape and size. The weld profile (Fig. 13b) shows good penetration without any defects.

Figure 14 shows typical hardness profiles of IF TWB across the weld line. The hardness profile was relatively flat across the weld metal itself, showing a very high hardness in the weld metal and the HAZ.

3.2 Comparison of Experimental and Predicted FLDs

The forming limit strain of IF TWB was predicted using six different necking criteria, namely SDT, ESR, MSR, TSR, TG, and NADDRG and compared with the experimental FLD as shown in Fig. 15. It is clear from Fig. 15 that FLD which was predicted by SDT is in closer agreement with the experimental results than other numerical FLD prediction methods.

Statistical analyses were used to assess the best order of the polynomial. Table 3 shows R^2 values for curve fitting of different FLD criteria. For all FLD criteria $R^2 > 0.9$ which indicate how well curves fit the data.

The limit strain values predicted near biaxial stretching conditions (strain paths: 150×200, 175×200, and 200×200 mm) by ESR, MSR, TSR, SDT, and TG are
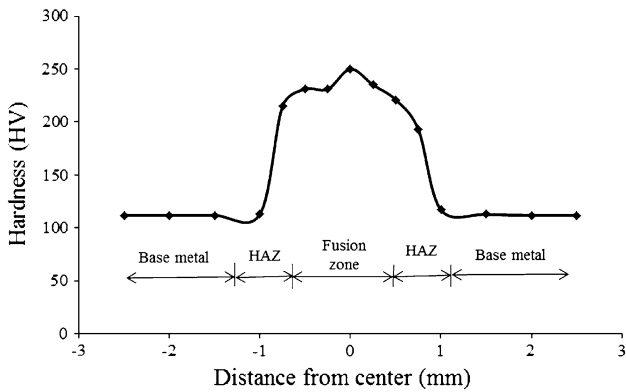
clustered within small strain values. The predicted FLDs by these numerical models are limited to the plane strain region and not grown to the extent expected normally on the stretching side. Figure 15 shows that numerical criteria cannot predict right-hand side of FLD and just proper for the left-hand side of FLD and plane strain condition.

It can be seen from comparison of the FLD which was predicted by NADDRG and experimental FLD that NADDRG model overestimates the limit strains for TWB. This result shows that NADDRG model has not good accuracy for FLD prediction of TWB. Although NADDRG can predict both the sides of FLD, its prediction is over experimental FLD which is in the fracture region and is not acceptable. SDT prediction limits to the left-hand side and plane strain condition of FLD, but its prediction is near experiment and in the safe region. Therefore, SDT model is more reliable than NADDRG which is located in the fracture region. Three FLDs criteria which were predicted by MSR, TSR, and TG are near to each other and located between ESR and SDT.

3.3 Necking Position Comparison

Figure 16 shows that TWB specimens with different widths yield different limit dome heights (LDHs). For experiment and also numerical criteria least of dome height was occurred for 125 mm width sample. This figure showed that minimum of LDH was happened in the plan strain condition. This result is agreed with Hosford and Caddel (Ref 26) result which notified that minimum of dome height is happened for sample in the plane strain condition.

Figure 17 shows the comparison between predicted failure location by SDT criterion and experimental results. In this

Fig. 14 Vickers hardness profile across the weld zone

Table 3 R^2 for different FLD criteria

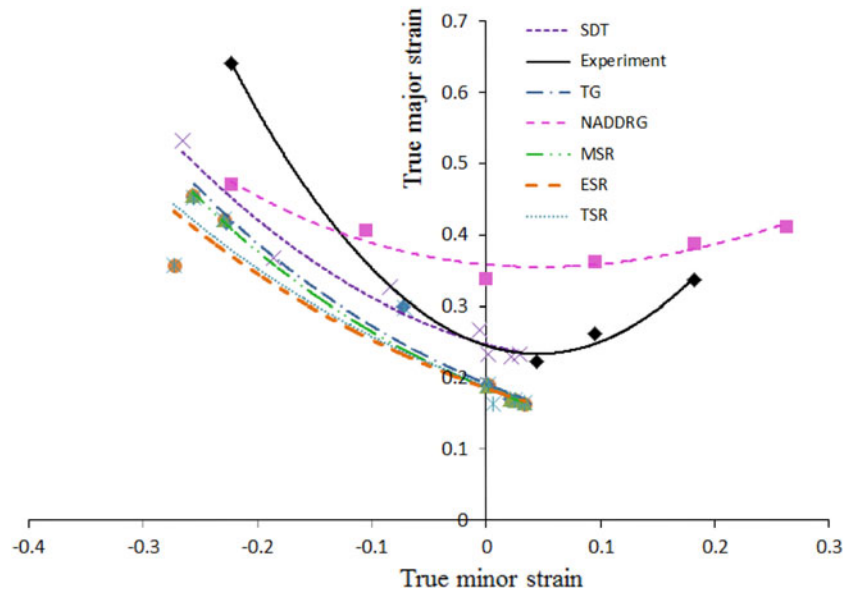| FLD criteria	TSR	MSR	ESR	SDT	TG	NADDRG	Experimental
R^2	0.997	0.989	0.997	0.970	0.999	0.930	0.997

Fig. 15 FLD comparison of IF TWB using different numerical criteria

figure, distance between weld line and failure position is shown by X parameter. Table 4 shows failure location comparison of experiment a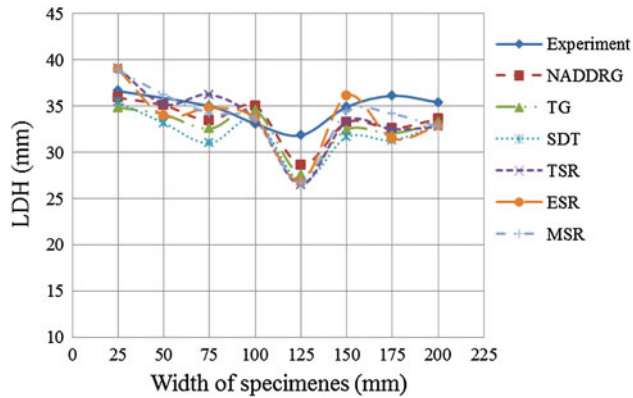nd FEM result and its error for different strain paths. It is clear from Fig. 17 and Table 4 that the failure locations predicted using the SDT criterion are in good agreement with experimental observations for varied strain paths and also X is decreased by sample width increasing.

4. Conclusions

In transverse tensile test (ASTM-E8) and also standard ball punch test of IF TWB with different thicknesses, it was found

Fig. 16 LDH variation with sample width for different FLD criteria

Table 4 Comparison of experiment and FEM results for distance between weld line and failure position (X)

Strain path	X, mm, experiment	X, mm, FEM	Error, %
25 × 200 mm	15.5	16.2	0.05
125 × 200 mm	4.4	4.32	0.02
200 × 200 mm	4	3.74	0.07

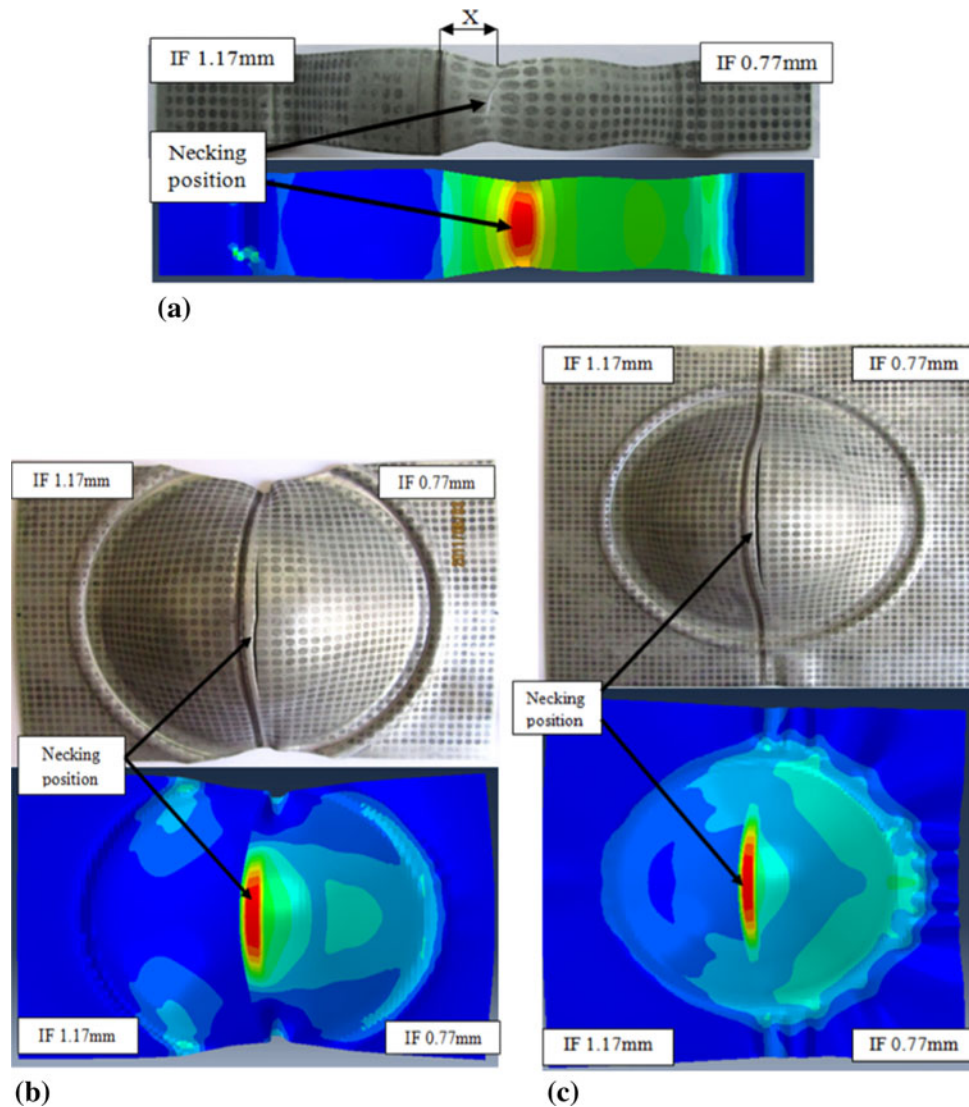**Fig. 17** Failure position comparison of experiment and FE for (a) 25 × 200 mm strain path, (b) 125 × 200 mm strain path, and (c) 200 × 200 mm strain path

that fracture takes place in the thinner/weaker material but not in the weld if it is free from defects and welding parameters are selected correctly. This conclusion is confirmed by considering microstructure of TWB which shows good penetration of weld.

Between numerical models of ESR, MSR, TSR, SDT, TG, and empirical model of NADDRG which were used for prediction of FLD of TWB, SDT has the best accuracy. Comparison of the FLD which was predicted by NADDRG, ESR, and experimental FLD shows that NADDRG model overestimates the limit strains for TWB and ESR underestimates.

The FLD predicted near biaxial stretching conditions by numerical criteria are clustered within small strain values such that the FLD on the stretching side is not grown to the extent expected normally. Therefore, numerical FLD criteria are not proper for prediction of right-hand side of FLD.

TWB specimens with different widths yield in different dome heights, so the LDH test scatter depends on the variation of the strain path at the fracture location. For experiment and also numerical criteria least of dome height is happened for 125 mm width sample that is in the plan strain condition.

Fracture position comparison of FEM and experiment show that there is good agreement for fracture position predicted by SDT criterion and experiment. Results show that by sample's width increasing or in the biaxial stretching condition, fracture occurs closer to the weld line.

References

1. Z.Q. Sheng, Formability of Tailor-Welded Strips and Progressive Forming Test, *J. Mater. Process. Technol.*, 2008, **205**, p 81–88
2. S.P. Keeler and W.A. Backofen, Plastic Instability and Fracture in Sheets Stretched Over Rigid Punches, *Trans. ASM*, 1963, **56**, p 25–48
3. G.M. Goodwin, Application of Strain Analysis to Sheet Metal Forming Problems in the Press Shop. SAE paper, 1968. Paper No.680093
4. S.S. Hecker, A Simple Forming Limit Curve Technique and Results on Aluminum Alloys, Sheet Metal Forming And Formability, *Proceedings of the 7th Biennial Congress of the International Deep Drawing Research Group, Amsterdam*, 1972, p 5.1–5.8
5. Z. Marciniak and K. Kuczynski, Limit Strains in the Processes of Stretch-Forming Sheet Metal, *Int. J. Mech. Sci.*, 1967, **9**, p 609–620
6. H.W. Swift, Plastic Instability Under Plane Stress, *J. Mech. Phys. Solids*, 1952, **1**, p 1–18
7. R. Hill, On Discontinuous Plastic States, With Special Reference to Localized Necking in Thin Sheets, *J. Mech. Phys. Solids*, 1952, **1**, p 19–30
8. Z. Marciniak, K. Kuczynski, and T. Pokora, Influence of the Plastic Properties of a Material on the Forming Limit Diagram for Sheet Metal in Tension, *Int. J. Mech. Sci.*, 1973, **15**, p 789–805
9. K. Narasimhan and R.H. Wagoner, Finite Element Modeling Simulation of In-Plane Forming Limit Diagrams of Sheets Containing Finite Defects, *Metall. Trans. A*, 1991, **22A**, p 2655–2665
10. R. Brun, A. Chambard, M. Lai, and P. de Luca P. Actual and Virtual Testing Techniques for a Numerical Definition of Materials, *Proc NUMISHEET'99. Besançon France*, 1999, p 393–398
11. T. Pepelnjak, A. Petek, and K. Kuzman, Analysis of the Forming Limit Diagram in Digital Environment. *Sheet Metal Erlangen, Germany* 5–8 April, 2005, p 697–704
12. M.F. Shi, K.M. Pickett, and K.K. Bhatt, Formability Issues in the Application of Tailor Welded Blank Sheet, *Proceedings of the Sheet Metal and Stamping Symposium*, 1993, p 27–35
13. M.F. Shi, M. Eisenmenger, and K.K. Bhatt, Influence of Laser Welding Parameters on Formability and Robustness of Blank Manufacturing: An Application to a Body Side Frame. SAE technical paper, 1995, Paper No. 950922
14. W.Y. Chien, J. Pan, and P.A. Friedman, *Int. J. Damage Mech.*, 2003, **12**, p 193–223
15. W.Y. Chien, J. Pan, and S.C. Tang, A Combined Necking and Shear Localization Analysis for Aluminum Alloys Sheets Under Biaxial Stretching Conditions. *Int. J. Plasticity*, 2004, **20**, p 1953–1981
16. L.C. Chan, S.M. Chan, C.H. Cheng, and T.C. Lee, Formability and Weld Zone Analysis of Tailor-Welded Blanks for Various Thickness Ratios, *J. Eng. Mater. Technol. Trans. ASME*, 2005, **127**, p 179–185
17. Metals Test Methods and Analytical Procedures, Annual Book of ASTM Standards, ASTM-E8 and ASTM-E517, West Conshohocken, PA Vol 03.01, 2000
18. Metals Test Methods and Analytical Procedures, Annual Book of ASTM Standards, ASTM-E643, West Conshohocken, PA, Vol 03.01, 2000
19. S.S. Hecker, A Cup Test for Assessing Stretchability, *Met. Eng. Q.*, 1974, **14**, p 30–36
20. F.I. Sunders, Forming of Tailor Welded Blanks. Ph.D. dissertation, Ohio State University, Columbus, OH, 1995
21. R. Safdarian, H. Moslemi Naeini, and G.H. Liaghat, Investigation of Weld Line Movement in Tailor Welded Blank Forming. AMPT2011, Istanbul, Turkey
22. R. Hill, A Theory of Yielding and Plastic Flow of Anisotropic Metals. *Proc. Roy. Soc. Lond.*, 1948, **193A**, p 197–281
23. Abaqus User Guide, ABAQUS Analysis User's Manual
24. S. Kumar, P.P. Date, and K. Narasimhan, A New Criterion to Predict Necking Failure Under Biaxial Stretching, *J. Mater. Process. Technol.*, 1994, **45**, p 583–588
25. S.B. Levy, A Comparison of Empirical Forming Limit Curves for Low Carbon Steel with Theoretical Forming Limit Curves of Ramaekers and Bongaerts, IDDRG WG3, Ungarn, 1996
26. W.F. Hosford and R.M. Caddel, *Metal Forming—Mechanics and Metallurgy*, 2nd ed., Prentice Hall, Englewood Cliffs, 1993